International Journal of Advance Research and Innovation
Vol. 1(3), Jul-Sept 2015, pp. 34-44
Doi: 10.51976/ijari.331506
www.gla.ac.in/journals/ijari


**Article Info**
Received: 03 Jul 2015 | Revised Submission: 20 Jul 2015 | Accepted: 28 Aug 2015 | Available Online: 15 Sept 2015

# Rigid Plastic Analysis of Metal Parts using Meshless Approach

*Ajay Chhillar*, Rajender Singh***

## ABSTRACT

*Plastic deformation of metal parts has been a matter of concern for investigators in academia, industry and research institutions all over the world. Literature reveals that earlier researchers have applied efforts for predicting plastic deformations using mesh based approach. A truly meshless formulation for rigid plastic analysis of metal parts has been developed in the present study for both plane stress and plane strain cases. In the present formulation, the governing equations are obtained for different set of scattered nodes over the problem domain and the integral equation for rigid plastic behavior is obtained through weak form over a local sub-domain. The meshless solution functions are obtained for different set of scattered nodes through moving least square technique. Essential boundary conditions are enforced through Penalty approach. The rigid plastic constitutive relationships incorporate only small deformation. Material constitutive relationship include Von-Mises yield criterion with rate independent associative flow theory. The solution algorithm for rigid plastic analysis of metal parts using meshless approach is discussed in the present work. Numerical results have been computed through two test functions using both linear and quadratic basis function which shows that presented formulation is accurate and robust for carrying out the rigid plastic analysis of metal parts.*

***Keywords:*** *Meshless Method; Rigid Plastic; Perfect Plastic; Truly Meshless; Meshless Local Petrov Galerkin Method.*

## 1.0 Introduction

Plastic deformation of metal parts has been a vital activity in the area of solid mechanics and has been carried out all over the world. Numerous techniques were used to find plastic deformation of metal parts and most popular technique is Finite Element Methods (FEM) till last decade. The meshless method possesses numerous merits over the FEM as stated by many researchers [1], [2], [3], [4], [5], [6], [7], [8], [9], [10]. Most of the pioneer's working in the area of meshless methods criticize FEM which motivated the others researchers to alleviate the problems arising due to mesh. Continuous efforts of these researchers inspired others to use some good features of FEM and they started generating system equations over the nodes in spite of element/mesh. The major progress towards the development of meshless methods started after the introduction of Diffuse Element Method (DEM) as reported by Nayroles in 1992 [11]. Later on, many meshless methods were reported in literature but the methods are called although meshless but they are not truly meshless. They somehow need mesh either for interpolation or for integration purpose. But due to the elimination of mesh requirement, the so called meshless methods became cheap and flexible. Their flexibility extends further if the methods become truly meshless. Messless Local Petrov Galerkin (MLPG) method, Local Boundary Integral Equation (LBIE) method, Point Weighted Least Squares (PWLS) methods are reported as truly meshless methods as they do not need any mesh either for interpolation or for integration purpose.

In the last decade, truly meshless methods have been successfully implemented to solve numerous engineering and science problems as reported by Sladek [12]. M. H. Kagarnovin at el reported to implement element free Galerkin method for elasto-plastic stress analysis around a crack tip [13]. Y. T. Gu implement the local meshless approach for solving elasto-plastic analysis of solid using total deformation theory [14]. Y. P. Chen et al implemented meshless approach for rate independent large strain plasticity problem under high speed impact and contact situation [15]. Jianfeng Ma at el

**Corresponding Author: Department of Mechanical Engineering, DCRUST Murthal, Sonipat, Haryana, India (E-mail: aasc1981@gmail.com)*
***Department of Mechanical Engineering, DCRUST Murthal, Sonipat, Haryana, India*

applied Meshless integral approach to solve elastoplastic small deformation problem [16]. But in literature, the perfect plastic analysis through truly meshless method were not found addressed and the aim of the present work is to explore the implementation of truly Meshless method for carrying out perfect plastic analysis of metal parts. In this regard a relationship between the nodes over the domain and value of field variable is required to be built for which moving least square technique is used. And the moving least square scheme can be referred/ presented as under.

## 2.0 The Moving Least Square Approximation (MLS)

In meshless methods the algebraic system equations are established without predefining the mesh over the whole problem domain. In this meshless method nodes are spotted over the whole problem domain and boundary and at these points the value of the field variable is required to be calculated. A relationship between the spotted nodes over the domain and boundary and value of field variable is required to be built. Some technique is needed that can approximate the value of field variable at these spotted nodes. There are a number of techniques available in literature viz.

Shepard function after Donald Shepard in 1968 **[**17**]**, in 1981 Peter Lancaster and K. Salkaushas [**18**] generalize the Shepard function and introduced Moving Least Squares Method, in 1997 Babuska and Melenk reported Partition of Unity Method [**19**], Liu, Chang in 1996 presented Reproducing Kernel particle method [**20**], in 1995 Robert Schaback introduced Compactly Supported Radial Basis Function [**21**] and some other methods that establish the relationship are also available in literature. Some of the interpolation techniques are compared by K.Y. Lam at el **22**]. In order to make the current meshless formulation general, the approximation scheme ought to have high computational accuracy, low computational cost, computationally easy to implement and extend to multidimensional problems [**23, 24**]. The moving least squares (MLS) approximation may be one of such schemes that fulfill above requirements.

Hence MLS approximation is used in the current implementation and it can be referred from [**18**], [**3**], [**2**].

## 3.0 Meshless for Mulation and Solution for Perfect Plastic Analysis of Metal Parts

The perfect plastic analysis of metal parts having continuous domain *D.* and bounded by boundary L, can be performed using the following equilibrium equation

$$\sigma_{ij,j} + b_i = 0 \qquad (1)$$

Here a^ represents stress tensor, CJJJJ represents the partial derivative of stress tensor w.r.t. space coordinate, and bj represents body force acting on the deforming domain £1 The metal part problem domain is subjected to Dirichlet boundary conditions for the $a^{th}$ node lying on the boundary Lf is uf = uf. The Neumann conditions comprises of ajjJVj$^3$ = tf for the $a^{th}$ node lying on Lf boundary portion of L boundary. For specifying the natural boundary condition, $JVj^a$ represents the components of the local outward normal vector calculated for an arbitrary $a^{th}$ node that lies on the $L_t$ boundary. The local weak form of the equilibrium equation in present investigation, i.e. applicable to a small local domain bounded in the vicinity of $a^{th}$ node, can therefore be written as

$$\int_{\Omega_q^a} v_i^a \left(\sigma_{ij,j} + b_j\right) d\Omega - \alpha \int_{\Gamma_{qu}^a} v_i^a \left(u_i^a - \bar{u}_i^a\right) d\Gamma = 0 \qquad (2)$$

Where, $\Omega_q^a$ represents quadrature sub-domain of $a^{th}$ node. This sub-domain can have arbitrary number of nodes, vf is a test function for $a^{th}$ node and it can theoretically be any function. And a is the penalty parameter used to enforce dirichlet boundary conditions as the shape function obtained through MLS approximation method do not satisfy Kronecker delta property. Here, $L_{qu}$ represent the portion of the global boundary L where displacement boundary conditions are specified for $a^{th}$ node. In order to obtain the weak form of Eq. (2), integration by parts i.e. Green's theorem is used so as to shift the order of differentiation from stress term to test function and using Divergence theorem, the volume integral is converted into surface integral. The weak form of the equilibrium equation for $a^{th}$ node can be expressed as

$$\int_{\Gamma_q^a} \sigma_{ij} \mathcal{N}_j^a v_i^a \, d\Gamma - \int_{\Omega_q^a} \sigma_{ij} v_{i,j}^a \, d\Omega + \int_{\Omega_q^a} b_i^a v_{i,j}^a \, d\Omega - \alpha \int_{\Gamma_{qu}^a} v_i^a \left(u_i^a - \bar{u}_i^a\right) d\Gamma = 0 \qquad (3)$$

Here $\Gamma_q^a$ represents quadrature/local sub-domain boundary of a[th] node, $v_{i,j}^a$ : represents the space derivative of

is approximately equal to external applied load vector so that iteration process can be terminated. Here in the the test function defined for a[th]node. And $JVj^a$ is the j[th] component of the unit outward normal vector for a[th] node having the boundary $L_q$. The term a^ $M^a$ is known as traction vector at a[th] point on the surface Lf, offered due to tf real force that acts on the surface $L_{qt}$. The boundary Lf, of the local quadrature domain fif, is now composed of $L_{qt}$ $L_{qu}$ &$L_{qi}$.

Where $L_{qt}$ represents the boundary of local quadrature domain where the traction force is acting on boundary portion Lf, of a[th] node. $L_{qu}$ represent the boundary portion Lf, of local quadrature domain where the displacement boundary conditions are specified for a[th] node. $L_{qi}$ represents the boundary of local quadrature domain which does not intersect with the global boundaries L i.e. the internal boundary of local quadrature domain.

The local weak form of the equilibrium equation can therefore now be rewritten for a local quadrature domain of node a which is located within global domain *D.* and on global boundaries L i.e.

$$\Gamma_q^a = \Gamma_{qi}^a \cup \Gamma_{qu}^a \cup \Gamma_{qt}^a \qquad (4)$$

On substituting Eq. (4) in Eq. (3) i.e.

$$\int_{\Gamma_{qt}^a} \sigma_{ij} \mathcal{N}_j^a v_i^a \, d\Gamma + \int_{\Gamma_{qu}^a} v_i^a \sigma_{ij} \mathcal{N}_j \, d\Gamma - \int_{\Gamma_{qi}^a} v_i^a \sigma_{ij} \mathcal{N}_j^a d\Gamma -$$

$$\int_{\Omega_q^a} (v_{i,j}^a \sigma_{ij} - v_i^a b_i^a) \, d\Omega - \alpha \int_{\Gamma_{qu}^a} v_i^a (u_i^a - \bar{u}_i^a) d\Gamma = 0 \qquad (5)$$

Eq. (5) has become now valid for those nodes, over which some traction force is acting on some portion of global boundary and some displacement boundary conditions are specified on some portion of the global boundary.

Eq. (5) therefore further reduces to Eq. (6) which is valid for all nodes whose local boundaries do not intersect with global boundaries in which integral term with internal quadrature boundary Lfj becomes zero because vf test function is chosen in such a way that its value is zero at the boundary.

$$\int_{\Omega_q^a} (\sigma_{ij} - b_i^a) v_{i,j}^a \, d\Omega = 0 \qquad (6)$$

It is worthwhile to mention here that in the present formulation the integration is carried out over local quadrature sub-domains and if the whole problem domain is not covered then this formulation can generate numerical errors. In order to reduce such numerical errors, more accurate discretization of the problem is therefore required and due to this, the overlapping of sub-domains is allowed.

The local weak form of equilibrium equation as given by Eq. (5) and (6) are valid for continuous local sub-domain space of a[th] node.

This way the continuous problem space is discretized into a finite N number of nodes. The discretized problem domain for the continuous problem space can now be written as a set of nonlinear equations that represents the whole problem domain.

$$[K]\{U\} = \{F\} \qquad (7)$$

Here [K] is known as assembled stiffness matrix, {U} is known as global displacement field vector and {F} is known as global force vector. For solving this nonlinear eq. (7), the incremental iterative procedure with radial return method is used. For each iteration of loading step, the equilibrium is now checked whether the internal load vector present work for economy modified Newton Raphson scheme is applied.

The next step is to write various quantities on to the disc for post processing purpose.

In the above set of nonlinear equations, the contribution of a particular a[th] field node within the deforming space can therefore be represented as

$$[k_{ij}^a]\{u_j^b\} = \{f_i^a\} \qquad (8)$$

Where [kf:] represents a[th] nodal contribution to Global stiffness matrix and {f/[1]} represents the nodal force contribution to global force vector.

This contribution includes the body forces applied at the problem domain of a[th] node, traction force applied on boundary and penalty

force term. Here $\{u_j^b\}$ term represents the displacements caused in the adjacent b[th] nodes when force is applied at a[th]node and adjacent b[th] nodes lie within the influence domain of a[th]node. It is also to be noted here that the adjacent b[th] nodes are variables and they vary from node number 1 to n. Where n, is total number of nodes within influence domain of a[th]node. The term $k_{ij}^{a,b}$ represents stiffness contribution of a particular a[th] node to one of the specific adjacent b[th] node within influence domain of a[th] node.

$$[k_{ij}^a]_{2\times 2n}\{u_j^b\}_{2n\times 1} =$$

$$\int_{\Omega_q^a}\begin{bmatrix}\frac{\partial v^a}{\partial x} & 0 & \frac{\partial v^a}{\partial y}\\ 0 & \frac{\partial v^a}{\partial y} & \frac{\partial v^a}{\partial x}\end{bmatrix}_{2\times 3}[D_p]_{3\times 3}\begin{bmatrix}\frac{\partial \theta_1}{\partial x} & 0 & \frac{\partial \theta_2}{\partial x} & 0 & \dots & \frac{\partial \theta_n}{\partial x} & 0\\ 0 & \frac{\partial \theta_1}{\partial y} & 0 & \frac{\partial \theta_2}{\partial y} & \dots & 0 & \frac{\partial \theta_n}{\partial y}\\ \frac{\partial \theta_1}{\partial y} & \frac{\partial \theta_1}{\partial x} & \frac{\partial \theta_2}{\partial y} & \frac{\partial \theta_2}{\partial x} & \dots & \frac{\partial \theta_n}{\partial y} & \frac{\partial \theta_n}{\partial x}\end{bmatrix}_{3\times 2n}\begin{Bmatrix}u_x^1\\ u_y^1\\ u_x^2\\ u_y^2\\ \vdots\\ u_x^n\\ u_y^n\end{Bmatrix}_{2n\times 1} d\Omega +$$

$$\int_{\Gamma_{qu}^a}\begin{bmatrix}v^a & 0\\ 0 & v^a\end{bmatrix}_{2\times 2}[N^a]_{2\times 3}[D_p]_{3\times 3}\begin{bmatrix}\frac{\partial \theta_1}{\partial x} & 0 & \frac{\partial \theta_2}{\partial x} & 0 & \dots & \frac{\partial \theta_n}{\partial x} & 0\\ 0 & \frac{\partial \theta_1}{\partial y} & 0 & \frac{\partial \theta_2}{\partial y} & \dots & 0 & \frac{\partial \theta_n}{\partial y}\\ \frac{\partial \theta_1}{\partial y} & \frac{\partial \theta_1}{\partial x} & \frac{\partial \theta_2}{\partial y} & \frac{\partial \theta_2}{\partial x} & \dots & \frac{\partial \theta_n}{\partial y} & \frac{\partial \theta_n}{\partial x}\end{bmatrix}_{3\times 2n}\begin{Bmatrix}u_x^1\\ u_y^1\\ u_x^2\\ u_y^2\\ \vdots\\ u_x^n\\ u_y^n\end{Bmatrix}_{2n\times 1} d\Gamma + \qquad (9)$$

$$\alpha\int_{\Gamma_{qu}^a}\begin{bmatrix}v^a & 0\\ 0 & v^a\end{bmatrix}_{2\times 2}\begin{bmatrix}\phi_1 & 0 & \phi_2 & 0 & \dots & \phi_n & 0\\ 0 & \phi_1 & 0 & \phi_2 & \dots & 0 & \phi_n\end{bmatrix}_{2\times 2n}\begin{Bmatrix}u_x^1\\ u_y^1\\ u_x^2\\ u_y^2\\ \vdots\\ u_x^n\\ u_y^n\end{Bmatrix}_{2n\times 1} d\Gamma$$

For the particular a[th] node that lies on or nearer to the boundary of global domain, the above local weak form of equilibrium equation after separating the known and unknown variables can now be written in discretized form as above

$$\{f_i^a\}_{2\times 1} = \int_{\Gamma_{qu}^a}\begin{bmatrix}v^a & 0\\ 0 & v^a\end{bmatrix}_{2\times 2}\begin{Bmatrix}\bar{t}_x\\ \bar{t}_y\end{Bmatrix}_{2\times 1} d\Gamma + \alpha\int_{\Gamma_{qu}^a}\begin{bmatrix}v^a & 0\\ 0 & v^a\end{bmatrix}_{2\times 2}\begin{Bmatrix}\bar{u}_x^a\\ \bar{u}_y^a\end{Bmatrix}_{2\times 1} d\Gamma + \int_{\Omega_q^a}\begin{bmatrix}v^a & 0\\ 0 & v^a\end{bmatrix}_{2\times 2}\begin{Bmatrix}b_x^a\\ b_y^a\end{Bmatrix}_{2\times 1} d\Omega \qquad (10)$$

Where adjacent b[th] node is varying from 1 to n. Here n is total number of nodes within the influence domain of a[th] node and $[D_p]$ is perfect plastic material constitutive matrix in Eq. (9). Here $[\ ^a]$ in Eq. (9) represents the unit outward normal matrix for a[th] field node that lies on the boundary $r_q{}^a{}_u$. The unit outward normal matrix

$$[\ ^a] = \begin{bmatrix} {}^a_x & 0 & {}^a_y \\ 0 & {}^a_y & {}^a_x \end{bmatrix} \qquad (11)$$

Where $_x$ & $_y$ represents the normal vector components along x and y direction respectively at a[th] node point that lies on the boundary $\Gamma_q{}^a{}_u$. Similarly above equations can therefore be obtained for a[th] field node that lie

entirely within global domain and their local quadrature domain do not intersect with global boundary.

### 4.0 Rigid Plastic Constitutive Relation

In Eq. (9), the $[D_p]$ matrix is required for solution and

this matrix represents perfect plastic constitutive relation. According to incremental flow theory the perfect-plastic constitutive relation requires three conditions for establishing correct stress – strain relationship. They are flow rule, yield condition, loading and unloading condition. According to incremental flow theory for small deformation analysis of metal the total strain increment

$d\{\epsilon_t\}$ can be next decomposed into two parts. Those are elastic strain $\{d\epsilon_e\}$ and plastic strain $\{d\epsilon_p\}$ in vector form.

$$\{d\epsilon_t\} = \{d\epsilon_e\} + \{d\epsilon_p\} \qquad (12)$$

The incremental stress strain relation can be further written as in matrix form as

$$\{d\sigma\} = [D_{ep}]\{d\epsilon_t\} \qquad (13a)$$

$$\{d\sigma\} = [D](\{d\epsilon_t\} - \{d\epsilon_p\}) \qquad (13b)$$

Eq. 13b is valid for [D] elastic deformation but for this evaluation plastic strain is required to be known and it must be a function of material. The incremental plastic strain magnitude and direction can be related to current stress state through flow rule.

$$\{d\epsilon_p\} = d\lambda\left\{\frac{\partial F}{\partial f\sigma 1}\right\} = d\lambda\{a\} \qquad (14)$$

In Eq. (14) F is yield function and this modeling theory is popularly known as Associated Theory of Plasticity.

Now applying the yield criterion to decide whether the material has yielded or not. The material's behavior which is idealized as elastic-perfectly plastic material is presented in Eq. (15)

$$F = f(\sigma) = k^2 \qquad (15)$$

On applying Von Mises yield criterion, the Eq. (15) can now be rewritten as

$$f = 0.5\,S_{ij}S_{ij} - k^2 = 0.5\,S_{ij}S_{ij} - \tfrac{1}{3}\sigma_e^2 = 0 \qquad (15b)$$

Here f represents yield function, $S_{ij}$ is deviatoric components of stresses, $\mathbf{a}_e$ is effective stress and is assumed here equal to yi for perfect plastic case H = 0 i.e. ($a_e$ = y + $Hs_p$). where H is hardening modulus and $\mathbf{s}_p$ is effective plastic strain. It is important to note here that f is fixed as no hardening is considered.

Now before substituting Eq. (15) into Eq. (14), it is to be checked whether state of stress lies on the yield surface. Such conditions are guaranteed by consistency conditions. These consistency conditions can be summarized as under and are sometimes referred as Kuhn-Tucker conditions

$$d\lambda \geq 0, \quad F \leq 0, \quad d\lambda F = 0 \qquad (16)$$

The first condition in Eq. (16) states that plastic multiplier scalar cannot be negative; the second condition signifies that the state of stress at any point within the specimen can lie on or within the yield surface. The last condition states that during plastic deformation the state of stress always lies on the yield surface.

From Kuhn- Tucker 3rd condition that during plastic deformation when specimen is loaded or unloaded, a change in yield function occurs and it can mathematically be represented as

$$d\lambda dF = 0 \text{ if } F = 0 \quad (17)$$

Once the plastic deformation occurs then it is irrecoverable hence d**X** cannot be equal to zero so dF must be equal to zero.

$$\frac{dF}{d\{\sigma\}} d\{\sigma\} = 0 \quad (18)$$

Substituting Eq. (13b) and Eq. (14) into Eq. (18) it will lead to Eq. (19)

$$\{a\}^T[D](\{d\epsilon_t\} - \{d\epsilon_p\}) = 0 \quad (19)$$

Now replacing $\{d\epsilon_p\}$ as in Eq. (19) with Eq. (14)

$$\{a\}^T[D](\{d\epsilon_t\} - d\lambda\{a\}) = 0 \quad (20)$$

$$\text{Here } d\lambda = \frac{\{a\}^T[D]\{d\epsilon_t\}}{\{a\}^T[D]\{a\}} \quad (21)$$

Now substituting Eq. (21) into Eq. (14) the magnitude of plastic strain components, can now be evaluated by Eq. (22)

$$\{d\epsilon_p\} = d\lambda \left\{\frac{\partial F}{\partial\{\sigma\}}\right\} = d\lambda\{a\} = \frac{\{a\}^T[D]\{d\epsilon_t\}}{\{a\}^T[D]\{a\}}\{a\} \quad (22)$$

Now substituting Eq. (22) into Eq. (13b)

$$\{d\sigma\} = [D]\left(\{d\epsilon_t\} - \left\{\frac{\{a\}^T[D]\{d\epsilon_t\}}{\{a\}^T[D]\{a\}}\{a\}\right\}\right) \quad (23)$$

On taking $\{d\epsilon_t\}$ as common factor, then Eq. (23) leads to Eq. (24)

$$\{d\sigma\} = \{d\epsilon_t\}\left[[D] - \left\{[D]\frac{\{a\}^T[D]}{\{a\}^T[D]\{a\}}\{a\}\right\}\right] \quad (24)$$

Now on comparing Eq. (24) to Eq. (13b), the term within square bracket should represent $[D_p]$ matrix. So the term within square bracket represents elasto-plastic constitutive relation for perfect plastic materials.

$$[D_p] = \left[[D] - \left\{[D]\frac{\{a\}^T[D]}{\{a\}^T[D]\{a\}}\{a\}\right\}\right] \quad (25)$$

Note that Eq. (25) contains plastic multiplier and flow vector, however dλ is also a function of flow vector which makes Eq. (25) nonlinear and it incorporates only material nonlinear behavior which has been validated as under.

## 5.0 Validation of Rigid Plastic Meshless Formulation: Results and Discussion

Two case studies namely thick cylindrical pressure vessel subjected to internal pressure and an infinite plate with a circular hole subjected to continuously increasing traction along Y axis are presented for validation of above Meshless formulation.

### 5.1. Case study of thick cylinder subjected to continuously increasing pressure

The problem domain of long thick cylinder is discretized into 861 nodes with regular nodal distribution of 21x41 with . ° along theta direction and 0.25 units spacing in radial direction. The discretized geometry of thick cylinder subjected to continuously increasing pressure is presented through Figure. 1.

Owing to symmetry in geometry and loading conditions only upper right segment of cylinder is modeled. The problem domain is modeled as plane strain. The internal radius of the cylinder is 5m and outer radius of the cylinder is 10m. The material of the cylinder has young's modulus of 210.8 GPa, Poisson's ratio of 0.3, yield strength of 0.2002 GPa and zero hardening modulus. The imposed boundary conditions for the quarter segment of thick cylinder comprises of displacement along X direction is restricted for the left face while this face is free to move along Y direction; the bottom face is restricted to move along Y direction and it has no restriction to move along X direction. The traction boundary conditions are specified on inner radius and no traction is specified on the outer radius of the cylinder. The problem is solved using Gaussian Test Function (GTF) both for linear basis function (LBF) and quadratic basis function (QBF). During testing, the internal pressure of the cylinder is increased from 0 to 131.875 MPa in 5 load steps and the load steps are kept same as applied

by Abaqus student version software. The initial yielding is observed at 115 MPa loading.

**Fig: 1. Discretized Geometry, Loading and Boundary Conditions of Cylinder**

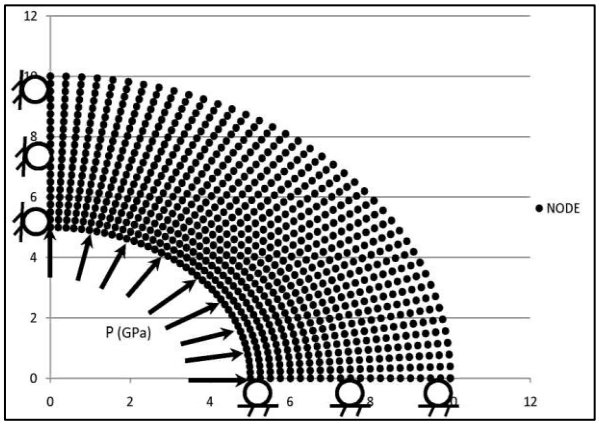

The comparison of Min. Principal Stress using Gaussian test function along Y=0 are represented through Fig.2a are with LBF and Fig.2b are with QBF. The comparison of Von Misses stresses distribution along Y=0 are represented through Fig.3a are with LBF and Fig.3b are with QBF. The spread of plastic zone as obtained from above presented formulation for different loading is presented for Gaussian Test Function are with LBF Fig.4a and Fig.4b is with QBF.

**Fig: 2a. Comparison of min. principal stress using GTF with LBF at 131.875MPa Internal Pressure**

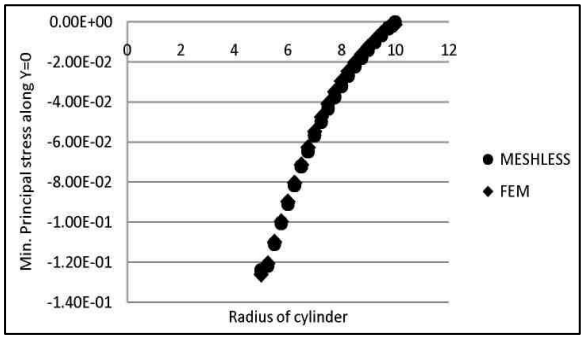


**Fig: 2b. Comparison of Min. Principal Stress Using GTF with QBF at 131.875MPa Internal Pressure**

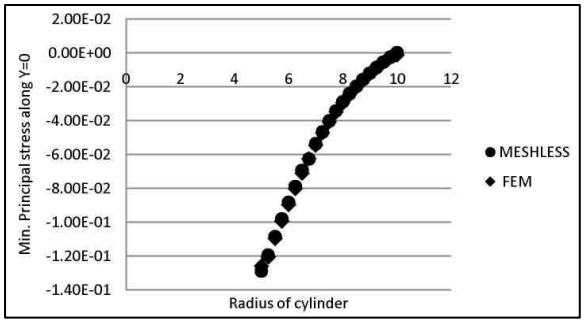


**Fig: 3a. Comparison of Von Mises Stress Using GTF with LBF at 131.875MPa Internal Pressure**

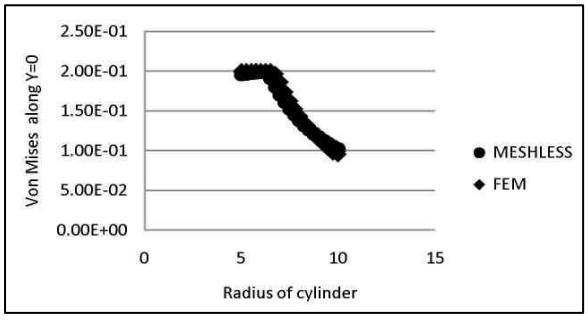


**Fig: 3b. Comparison of Von Mises Stress Using GTF with QBF at 131.875MPa Internal Pressure**

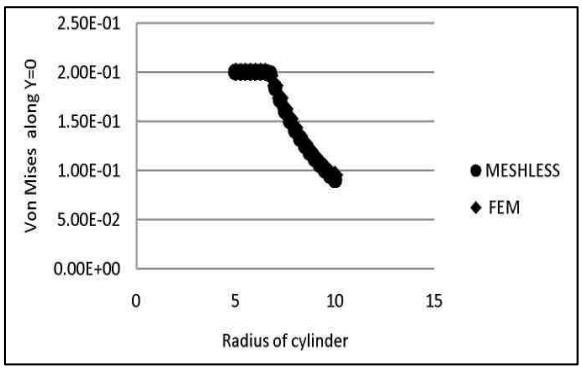


**Fig: 4a. Spreading of Plastic Strain Using GTF with LBF at 131.875MPa Internal Pressure**

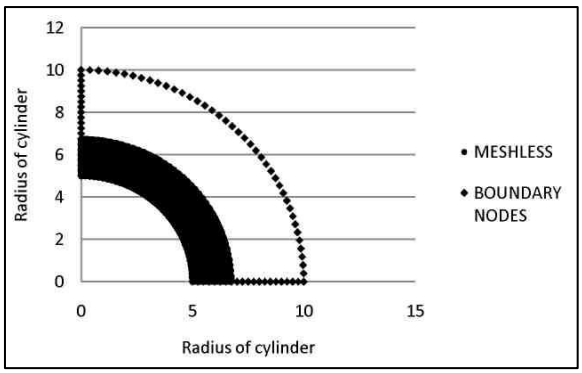


**Fig: 4b. Spreading of Plastic Strain Using GTF with QBF at 131.875MPa Internal Pressure**

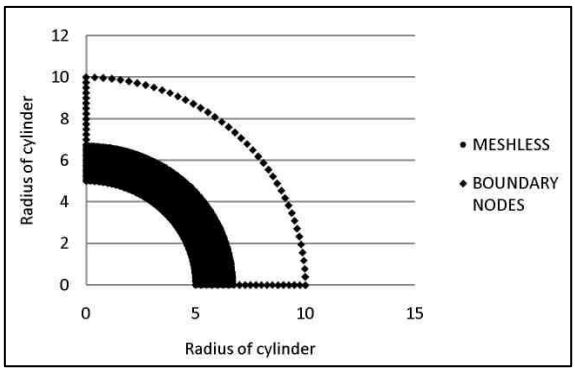


The undeformed and deformed shape is compared for 131.875 MPa internal pressure and are represented through Fig.5a with LBF and Fig.5b with QBF. In these figures the dot represents undeformed geometry; diamond represents deformed geometry obtained through meshless formulation while triangle

represents deformed geometry obtained through FEM based Abaqus student version software.

**Fig: 5a. Comparison of Deformed Meshless Model Using GTF and LBF at 131.875MPa Internal Pressure**

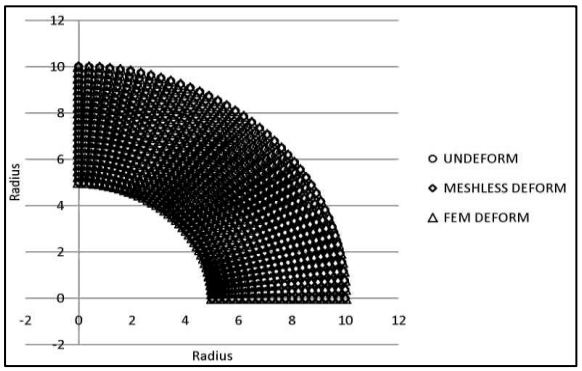


**Fig: 5b. Comparison of Deformed Meshless Model Using GTF and QBF at 131.875MPa Internal Pressure**

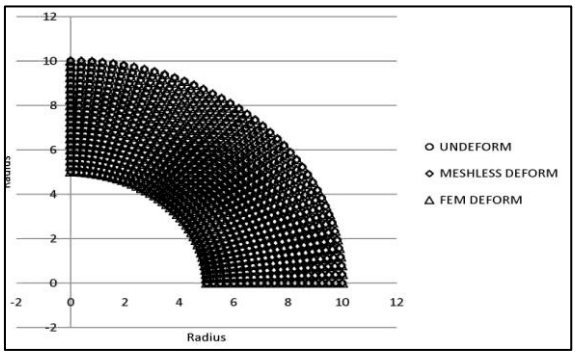


It can be observed from the above presented results when compared the results obtained through FEM based that meshless computational results are in good agreement Abaqus student version software.

### 5.2. Case study of infinite plate with central circular hole subjected to continuously increasing traction along Y axis

An infinite plate with a central circular hole subjected to normal traction along top and bottom is considered here for validating the presented formulation. Owing to symmetry in geometry and loading condition, only right upper quadrant is considered here as shown in Fig. 6. The plate is 50 m long and 50 m wide with 5m radius of hole. The quarter plate model is discretized with 863 nodes through Abaqus student version software and the same nodal data is used for validating current meshless formulation. The boundary conditions enforced over the quarter segment is presented in Fig.6. The Dirichlet boundary conditions are enforced over the left face and bottom face of the quarter segment. The left face is restrained along X direction while bottom face is restrained along Y direction. The left face is free to move along Y direction while the bottom face is free to move along X direction. The Neumann boundary condition is applied on the top face of quarter section along Y direction. The right face is a free boundary. The material properties of the test plate having young's modulus of 210.83 GPa, Poisson's ratio of 0.3, yield strength of 0.2002 GPa and hardening modulus is 0 GPa. During the testing the uniform normal traction along Y axis is increased from 0 to 154.375 MPa in 7 load steps.

The load steps are same as applied by Abaqus student version software. This problem is solved for Spline Test Function (STF) both with linear basis function and quadratic basis function. The variation of Von-Mises stress along Y=0 is computed and compared with Abaqus student software. The results are presented through Fig. 7a for LBF and in Fig.7b for QBF for 126.25Mpa traction along y axis. The deformed and undeformed shape is also presented in Fig.8a for LBF and in Fig.8b for QBF. The undeformed geometry is represented by circle and deformed geometry through FEM is represented by diamond whereas, the deformed geometry using the presented formulation is represented through triangle. The load steps are same as obtained through Abaqus student version software. And the first yielding behavior is observed at 70 MPa.

**Fig: 6. Discretization, Boundary Conditions and Loading Along Y Axis**

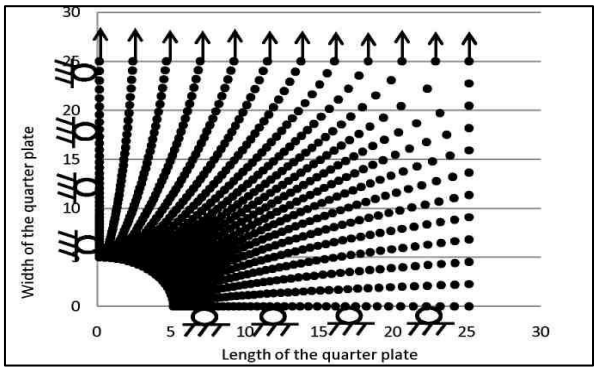

**Fig: 7a. Comparison of Von Mises Stress Using STF with LBF at 126.25Mpa Traction Along Y Direction**

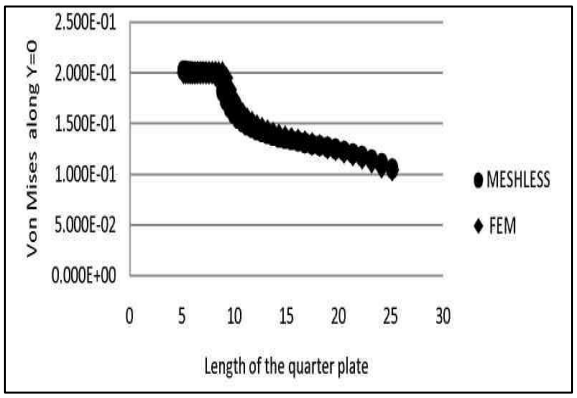


**Fig: 7b. Comparison of Von Mises Stress Using STF with QBF at 126.25Mpa Traction Along Y Direction**

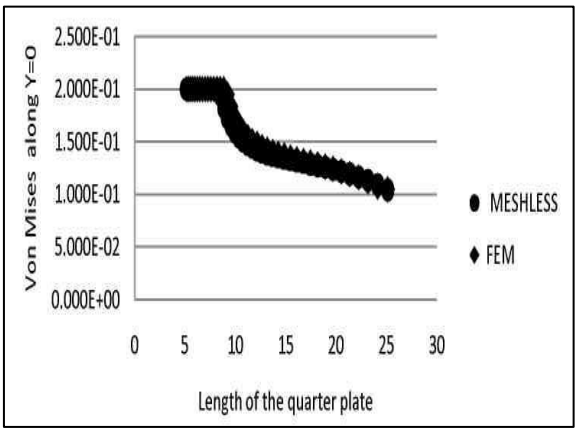


**Fig: 8a. Comparison of Deformed Meshless Model Using STF with LBF at 137.5MPa Traction Along Y Direction**

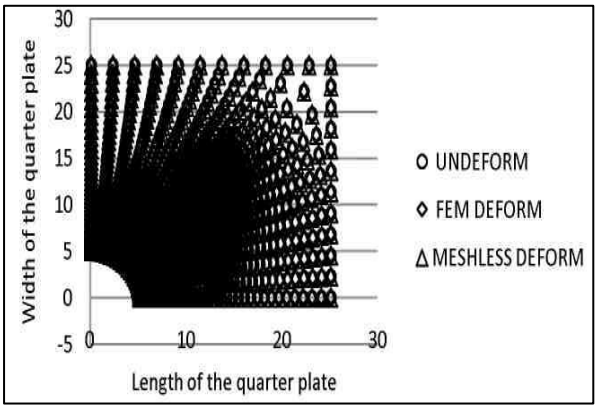


**Fig: 8b. Comparison of Deformed Meshless Model STF with QBF at 137.5MPa Traction Along Y Direction**

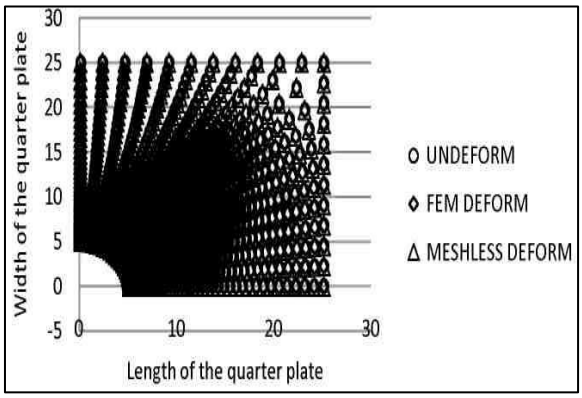


**Fig: 9a. Spreading of Plastic Strain Using STF-with LBF at 154.375 MPa Traction Along Y Direction**

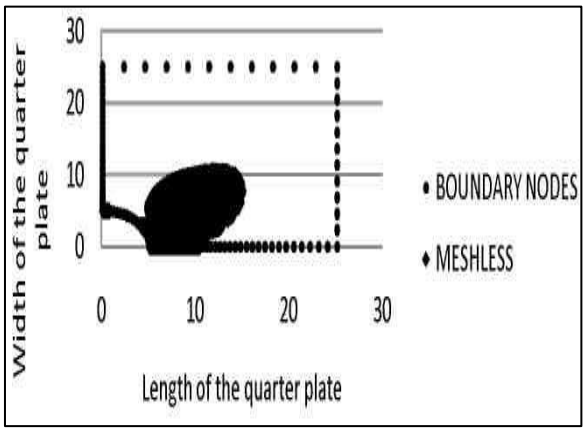


The effective plastic strain spread zone as obtained from above formulation using spline test function with LBF and QBF are represented in Fig. 9a and Fig. 9b respectively for 154.375 MPa. The variation of along Y=0 using spline test function is presented in Fig.10a for LBF and Fig.10b for QBF respectively corresponding to $6^{th}$ load step which is 137.5 MPa. Here it is quite lucid from Fig.7a and Fig.7b for Von Mises stress along Y=0 and from Fig.8a and Fig.8b that for deformed and undeformed shape, the results obtained from above formulation are in close agreement with the result obtained from FEM based Abaqus student version. The results in Fig.10a and Fig.10b represents along Y=0 and a slight deviation is observed near the hole with LBF. The deviation is reduced to a much greater extent

using QBF. The computed results can be still improved by using suitable sub-domain and support domain sizes.

**Fig 9b: Spreading of Plastic Strain Using STF with QBF at 154.375MPa Traction Along Y Direction**

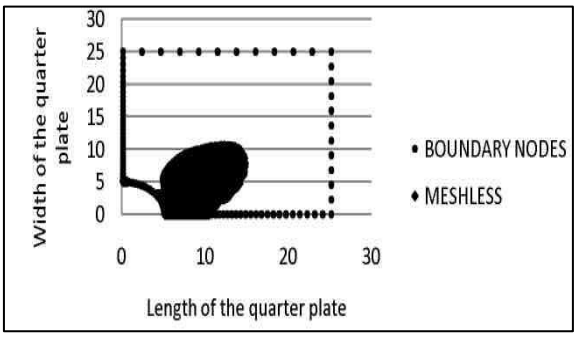


**Fig: 10a. Comparison of σ_YY Using STF with LBF at 137.5MPa Traction Along Y Direction**

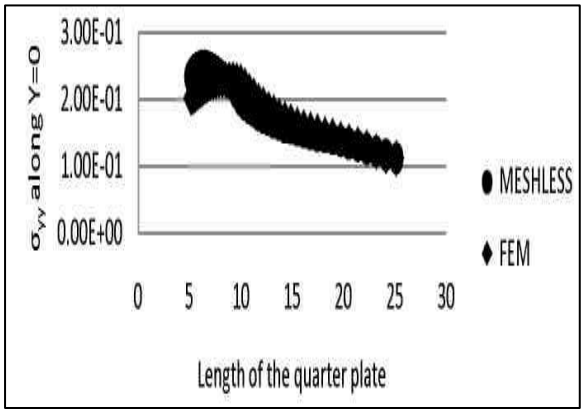


**Fig: 10b. Comparison of σ_YY Using STF with QBF at 137.5MPa Traction Along Y Direction**

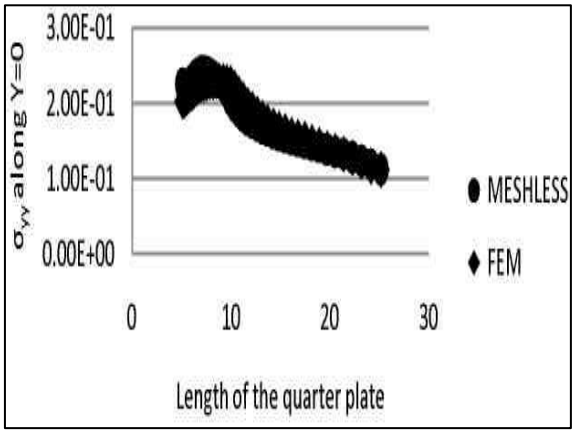


**6.0 Conclusion**

In this paper a true meshless approach is implemented for rigid plastic analysis of metal parts for plane stress and plane strain cases. In the present work, the governing equation are obtained for different set of sprinkled nodes over the problem domain and the integral equation are obtained through weak form of rigid plastic behavior over a local sub-domain. The meshless solution functions for different set of sprinkled nodes are obtained through moving least square technique. The essential boundary conditions are enforced through Penalty approach whereas no special attention is required to cater natural boundary conditions as they are automatically handled in the formulation. The constitutive relation implemented above incorporates only small deformation. The material constitutive relations are based upon rate independent flow theory with Von-Mises yielding condition. The nonlinear governing equations are solved using incremental iterative approach with modified Newton Rapsons technique because generating new stiffness matrix in each iteration is a costly affair. The numerical example case studies show that the above presented formulation is accurate and robust for modeling rigid plastic behavior of metal parts if suitable support and sub-domain sizes are chosen. It is further expected that MLPG method will soon replace FEM or BEM due to its high speed to convergence, good accuracy, and robustness

**Ackonowledgement**

The support provided for this research by Dr. Atul Kumar Aggarwal, Associate Professor, Department of Mechanical Engineering, Delhi Technological University Delhi, India is highly acknowledged. spaced points., 23rd ACM national conference, 68, New York, USA, 1968, 517-524

**References**

[1] S. S. Mulay, H. Li, *Meshless methods and their numerical properties*. New york: CRC press, 2013

[2] S. Verma, N. Yadav, A. Chhillar, Dynamic analysis of a centelever beam using MLPG method, mechanical engineering, C.R. State College of Engineering, Sonipat, India, 2006

[3] S. N. Atluri, The meshless method (MLPG) for domain & BIE discretizations. Forsyth, GA., USA: Tech science press, 2004

[4] S. Shen, S. N. Atluri, *The Meshless Local Petrov-Galerkin (MLPG) Method.*: Tech Science Press, 2002

[5] G. R. Liu, *Meshfree methods moving beyond the Finite Element Method*. Boca Raton, USA: CRC press, 2002

[6] M. B. Liu, G. R. Liu, Smooth partical hydrodynamics, a meshfree partical method. Toh Tuck Link, Singapore: World scientific publication Co. Pte Ltd, 2003

[7] W. K. Liu, S. Li, *Meshfree partical methods.* Berlin, Germany: Springer, 2004

[8] A. H. V. D. Boogaard, W. Quak, Nodal integration of meshless methods, International confrence on Partical Based Method, Barcelona, 2009, 1-4

[9] P. Pudjisuryadi, Adaptive meshless local petrov-galerkin method with Variable domain of influence in 2D elastostatic problems, Civil engineering dimension, 10(2), 2008, 99-108

[10] K. J. Bathe, S. De, Towards an efficient meshless computational technique: the method of finite spheres, Engineering Computations, 18(1/2), 2001, 170-192

[11] G. Touzot, P. Villon, B. Nayroles, Generalizing the Finite element method: diffuse approximation and diffuse elements., Computational Mechanics, 10(5), 1992, 307-318

[12] P. Stanak, Z. D. Han, V. Sladek, S. N. Atluri, J. Sladek, Applications of the MLPG Method in Engineering & Sciences: A Review, Computer modeling in engineering and sciences, 92(5), 2013, 423-475

[13] H. E. Toussis, S. J. Fabiborz, M. H. Kagarnovin, Elasto-plastic element free Galerkin Method, Computational Mechanics, 33, 2004, 206-214

[14] Y. T. Gu, An elasto-plastic analysis of solids by the local meshless method based on MLS, International Journal of Modern Physics B, 22(31/32), 2008, 5780-5786

[15] A. Eskandarian, M. Oskard, J. D. Lee, Y. P. Chen, Meshless analysis of high speed impact, Theoritical and Applied Fracture mechanics, 44, 2005, 201-207

[16] X. J. Xin, K. Prakash, J. Ma, Elastoplastic meshless integral method, Computer methods applied mech. Engrg., 197, 2008, 4774-4788

[17] D. Shepard, A two dimentional function for irregularly

[18] P. Lancaster, Salkauskas K., Surface generated by moving least square methods, Mathematics of Computation, 37(155), 1981, 141–158

[19] J. M. Melenk, I. Babuska, The partion of unity method, International Journal Numeriacl method engineering, 40(4), 1997, 727-758

[20] Y. Chen, R. Aziz Uras, C. T. Chang W. K. Liu, Generalized multiple scale reproducing Kernal partical methods, Computer Methods in Applied Mechanics and Engineering, 139(1-4), 1996, 91-157

[21] R. Schaback, Creating surfaces from scattered data using radial basis functions in mathematical methods for curves and surfaces, Mathematical methods for curves and surfaces, 477, 1995, 1-21

[22] Q. X. Wang, Li Hua, K.Y. Lam, A noval meshless approach- Local Kriging (LoKriging) method with two-dimentional structure analysis, computational mechanics, 33(3), 2004, 235-244

[23] T. Zhu S. N. Atluri, A new Meshless Local Petrov-Galerkin (MLPG) approach in computational mechanics, Computational Mechanics, 22, 1998, 117-127

[24] R. Cheng, Determination of a control parameter in a one dimensional parabolic equation using the moving least-square approximation, International Journal of Computer Mathematics, 85(9), 2008, 1363-1373